



Article citation info:

Plączek M, Kokot G, Degefa T, Subzero temperatures and low-frequency impact on MFC piezoelectric transducers for wireless sensor applications, *Eksploracja i Niezawodność – Maintenance and Reliability* 2024; 26(2) <http://doi.org/10.17531/ein/183316>

## Subzero temperatures and low-frequency impact on MFC piezoelectric transducers for wireless sensor applications

Indexed by:



Marek Łukasz Plączek<sup>a,\*</sup>, Tolera G. Degefa<sup>a</sup>, Grzegorz Kokot<sup>b</sup>,

<sup>a</sup>Department of Engineering Processes Automation and Integrated Manufacturing Systems, Silesian University of Technology, Poland

<sup>b</sup>Department of Mechanics and Computational Engineering, Silesian University of Technology, Poland

### Highlights

- Wireless sensors network reliability.
- Influence of temperature on energy harvesting systems.
- Macro Fiber Composite piezoelectric transducers applications.
- Mathematical modelling and laboratory tests of the system's efficiency and reliability.

### Abstract

This research paper is a continuation of a prior study [12] that focused on the positive temperature range. The current work investigates the behavior of a laminated Macro Fiber Composite (MFC) piezoelectric transducer when exposed to negative temperatures. The study aims to understand the sensitivity of the transducer under varying ambient temperatures and frequencies, particularly for applications in wireless sensor networks. The integrated Macro Fiber Composite piezoelectric transducer is both theoretically modeled and empirically verified. Experimental tests involve subjecting the laminated MFC piezoelectric transducer to sinusoidal forces generated by an electro-pulse waveform generator, while a thermal chamber is used for temperature control. Controlled displacement is applied to the transducer at low-frequency (5 to 25 Hz) ranges and different moderate temperatures (0 to -40 degrees Celsius). The results highlight the significant influence of temperature and excitation frequency on the generated voltage by the MFC transducer.

### Keywords

MFC piezoelectric transducer, WSN (wireless network sensors), FFT (fast furrier transformation), sensors, vibrational energy

This is an open access article under the CC BY license (<https://creativecommons.org/licenses/by/4.0/>)

### 1. Introduction

Smart composite materials, due to their potential for use as alternative energy sources and in autonomous wireless sensor systems, are becoming increasingly popular. The rising adoption of composite materials across various industrial sectors is driven by their versatile applications and potential benefits [2–6]. One such material is Macro Fiber Composite (MFC), which combines the advantageous properties of fiber and piezoelectric materials. MFC piezoelectric transducers have shown promise in harnessing vibrational energy for power generation, making them suitable for various applications,

(\*) Corresponding author.

E-mail addresses:

M.Plączek (ORCID: 0000-0002-5585-7621) [marek.placzek@polsl.pl](mailto:marek.placzek@polsl.pl), T. Degefa (ORCID: 0000-0003-0012-1681) [tolera.degefa@polsl.pl](mailto:tolera.degefa@polsl.pl), G. Kokot (ORCID: 0000-0002-5818-2869) [grzegorz.kokot@polsl.pl](mailto:grzegorz.kokot@polsl.pl)

including wireless sensor networks [1, 14, 16, 34]. This paper serves as a continuation of a previous study [12] that investigated the power generation capabilities of MFC piezoelectric transducers integrated with epoxy glass fiber composites in the positive temperature range. Building upon those findings, the present work aims to further explore the integration process and assess the power generation capacity of the transducers under varying ambient conditions.

Composite structures are increasingly popular in modern technical terms due to several advantages, notably high strength

at low weight. The use of this type of material creates new opportunities for engineers but poses a significant challenge due to the complex modeling processes required to ensure the proper operating parameters of the system, its durability, and reliability, with particular emphasis on structural fatigue caused by operational loads [17, 38]. Modern research methods allow the analysis and design of composite structures, considering these issues, among others, thanks to the use of machine learning tools and artificial intelligence [27, 28].

In the paper [40], we present and evaluate an energy harvesting device prototype with MFC patches on a cantilever beam to improve energy harvesting efficiency. We systematically investigate the impact of MFC electrical properties, cantilever beam configurations, and MFC geometric variations using FEA and EDA simulations. Piezoelectric materials possess a unique property: they generate electric charges when subjected to mechanical stresses and vice versa. This characteristic makes them ideal for designing transducers capable of converting electrical input signals into deformation and vice versa. It was demonstrated that the behavior of piezoelectric elements under different geometric configurations significantly influences their performance. Detailed discussions on the findings from the study on diverse geometric properties of piezoelectric transducers can be found in reference [10]. Optimizing the transducer's geometry has the potential to enhance energy harvesting, improve sensor performance, and enable precise actuation in micro-electromechanical systems (MEMS).

References [9–12] highlight the crucial role of piezoelectric transducers in structural health monitoring (SHM) by providing an efficient means of detecting and assessing structural integrity. These transducers, capable of converting mechanical strain into electrical signals and vice versa, offer exceptional sensitivity, compact size, and a wide frequency response. Their integration into SHM systems facilitates real-time monitoring, early detection of damage, and accurate evaluation of various structures, ranging from civil infrastructure to aerospace components.

Piezoelectric transducers have been extensively researched and utilized in Structural Health Monitoring (SHM), yet their potential for energy harvesting applications has garnered increasing interest. These transducers possess unique properties

that render them highly suitable for energy harvesting, extending beyond their traditional use in SHM. Capable of generating electric charges in response to mechanical stress or strain, piezoelectric transducers effectively convert various mechanical vibrations and deformations into electrical energy [44]. This distinct capability allows them to be employed across diverse energy harvesting scenarios, tapping into sources like human motion [14–16], environmental vibrations, and natural forces such as wind or ocean waves [17–19]. By harnessing ambient mechanical energy, piezoelectric transducers offer decentralized power generation opportunities, effectively capturing energy from otherwise wasted or underutilized sources.

These versatile transducers find integration in various applications and systems, including wireless sensor networks [20–23], wearable devices [24], self-powered electronics, and remote monitoring systems [7, 11, 15], among others. Furthermore, their adaptability to different environments and scalability enables deployment across a spectrum of settings, spanning from small-scale personal devices to extensive infrastructure. While the field of piezoelectric energy harvesting continues to evolve rapidly, substantial advancements have been achieved in transducer design, optimization, and power management techniques. Researchers have explored innovative approaches to enhance energy conversion efficiency, maximize power output, and improve overall performance of piezoelectric transducers in energy harvesting applications. Additionally, the integration of piezoelectric transducers with other renewable energy technologies and hybrid energy harvesting systems has shown promising results in maximizing energy generation and storage capabilities [27–29].

Piezoelectric transducers have demonstrated versatility across a wide spectrum of applications, encompassing structural health monitoring, energy generation, and sensing. However, their performance can be significantly affected by environmental factors, particularly temperature variations [1, 30, 31]. Understanding the impact of temperature on piezoelectric transducers is crucial, particularly in scenarios involving extreme temperatures. These transducers often encounter a broad temperature range in real-world applications, spanning from -40 degrees Celsius to 60 degrees Celsius or even higher. This range encompasses various conditions, from aircraft and

automotive systems to industrial settings, demanding reliable operation from piezoelectric transducers. Investigating their behavior across this temperature spectrum becomes imperative to enhance their performance and ensure their effective integration into diverse applications. The influence of temperature on piezoelectric transducers is intricate. Temperature fluctuations significantly alter the electrical properties of piezoelectric materials, including the piezoelectric coefficient, dielectric constant, and electrical conductivity. These changes directly impact the transducer's sensitivity, output voltage, and signal quality [5, 25, 33]. Moreover, temperature variations can affect the transducer's mechanical properties, such as stiffness, resonant frequency, and damping characteristics. Such fluctuations might impede the transducer's ability to efficiently convert mechanical vibrations into electrical energy or accurately detect and transmit mechanical signals.

This research delves into a comprehensive examination of the impact of temperature on piezoelectric transducers across a range from -40 to 60 degrees Celsius. By reviewing existing research, advancements, and challenges in this area, our goal is to contribute to understanding temperature-related issues and develop strategies to optimize piezoelectric transducer performance in extreme temperature environments. This understanding is vital for successful integration into applications where reliable operation in diverse temperature conditions is essential. The study aims to assess the power generation and sensitivity of transducers across various temperatures and frequencies, aiming to harness ambient vibrational energy for low-energy-consuming electronic systems and wireless sensor networks. Conducted in a controlled laboratory environment using a thermal chamber and electro-pulse waveform generator, our experimental setup applied a sinusoidal load to the integrated MFC transducer, inducing controlled displacements at low frequencies.

The results demonstrated a substantial influence of both excitation frequency and temperature changes on the voltage generated by the MFC transducer. Understanding these effects is critical for optimizing power generation capabilities and designing efficient ambient energy harvesting systems. Ultimately, this research advances the development of integrated MFC piezoelectric transducers for ambient energy

harvesting in wireless sensor networks. By exploring their capabilities under varying ambient conditions, this study opens avenues for sustainable power generation and lays the groundwork for energy-efficient wireless sensor networks.

## 2. Materials and methods:

The paper [12] provides a comprehensive explanation of the mathematical model used to analyze the impact of temperature and low frequency on a MFC piezoelectric transducer. The model assumes that the composite structure undergoes minimal deformations and exhibits linear material behavior. To simulate the transverse vibration force occurring in the laminated piezoelectric beam, an Instron Electro Pulse waveform generator was employed, applying the force at the center of the beam over both time and space. The dynamic behavior of the system is governed by a partial differential equation, which can be expressed as follows:

$$EI(x) \frac{\partial^4 u}{\partial x^4}(x, t) + (\rho A) \frac{\partial^2 u}{\partial t^2}(x, t) = \delta \left( x - \frac{l}{2} \right) F_o(t). \quad (1)$$

The transverse displacement is represented by  $u$ , the mass density of the beam is represented by  $\rho$ , the cross-sectional area of the composite beam is represented by  $A$ ,  $\delta$  is the Dirac delta function, which describes the dynamic load  $F_o(t)$  applied to the beam at the middle of the span and  $M$  is the internal bending moment. The presence of Equation (1) poses a challenge in finding an analytical solution due to its nature as a partial differential equation. Finding an explicit solution to this equation proves to be a complex task. However, in this case, an effective strategy to overcome this challenge is employed by employing the separation approach, also known as superposition. Given the inherent difficulty in directly solving Equation (1) analytically, the separation approach (equation (2)) provides a practical and viable method to tackle the problem at hand. By employing this technique, the equation is split into separate parts or components, each representing a distinct aspect of the problem. These components are then solved individually, considering the specific conditions and constraints of the system:

$$u(x, t) = \sum_{m=1}^{\infty} \varphi_k(x) \eta_k(t). \quad (2)$$

The function  $\varphi_k(x)$  plays a crucial role in the equation under consideration, representing the eigenfunction associated with the  $k$  -  $th$  vibration mode. The eigenfunction of a system defines its natural frequency and depicts the specific shape and

behavior of the mode. Analytical methods, like solving the homogenous solution of the laminated MFC piezoelectric transducer vibration, can be used to determine  $\varphi_k(x)$  and understand the distinct characteristics of each vibration mode. Alongside the spatial aspect represented by  $\varphi_k(x)$  the modal mechanical response  $\eta_k(t)$  describes how the  $k$ -th mode changes over time, considering factors like damping and external influences. Understanding  $\eta_k(t)$  allows us to observe how the vibration modes of the system respond to various stimuli. Together,  $\eta_k(t)$  and  $\varphi_k(x)$  provide a comprehensive representation of the  $k$ -th vibration mode. By combining these components, ones can analyze and predict the behavior of the mode in response to various conditions and input signals. It is worth noting that obtaining the analytical solution for  $\varphi_k(x)$  and  $\eta_k(t)$  can be a demanding task, often requiring advanced mathematical techniques. However, once determined, these solutions offer valuable insights into the system's dynamics and allow for a deeper understanding of the behavior exhibited by each vibration mode:

$$\varphi(x) = A \sin \beta x + B \cos \beta x + C \sinh \beta x + D \cosh \beta x, \quad (3)$$

where:  $\beta_k^2 = \omega \sqrt{\frac{\rho A}{EI}}$ .

The spatial component of the solution is expressed by Equation (3), providing the general solution for  $\varphi_k(x)$ . The constants A, B, C, D are of utmost importance in defining the shape and features of the spatial component. To find the values of these integration constants, boundary conditions must be considered. For a simply supported beam, specific conditions are applied at the support ends, which influence the behavior and shape of the mode shape functions, leading to a more precise solution. The general solution provided by Equation (3) allows for the customization of the spatial component, providing a versatile framework to capture the behavior and characteristics of the system under investigation. The boundary conditions at the ends of support implies the following conditions on mode shape functions:

$$\begin{aligned} \varphi(0) = \varphi(l) = 0, \\ \frac{d^3 \varphi(0)}{dx^3} = \frac{d^3 \varphi(l)}{dx^3} = 0. \end{aligned} \quad (4)$$

The coefficient of modal function is given by:

$$\begin{aligned} D - B = 0, C - A = 0, \\ -A\beta^2 \sin \beta l - B\beta^2 \cos \beta l + C\beta^2 \sinh \beta l \\ + D\beta^2 \cosh \beta l = 0, \end{aligned} \quad (5)$$

$$-A\beta^3 \cos \beta l + B\beta^3 \sin \beta l + C\beta^3 \cosh \beta l + D\beta^3 \sinh \beta l = 0.$$

Equation (5), can be arranged in matrix form:

$$\begin{bmatrix} \sinh \beta l - \sin \beta l & \cosh \beta l - \cos \beta l \\ \cosh \beta l - \cos \beta l & \sin \beta l + \sinh \beta l \end{bmatrix} \begin{bmatrix} A \\ B \end{bmatrix} = \begin{bmatrix} 0 \\ 0 \end{bmatrix}. \quad (6)$$

For a non-trivial solution, the determinant of the matrix must vanish to get:

$$\cosh(\beta_k l) \cos(\beta_k l) = 1. \quad (7)$$

This nonlinear equation can be solved numerically. The first four roots are  $\beta_1 l = 1.505\pi, \beta_2 l = 2.49975\pi, \beta_3 l = 3.5\pi, \beta_4 l = 4.5\pi$ .

The boundary conditions can also be used to determine the mode shapes from the solution for displacement:

$$\varphi(x) = [\sinh(\beta_k x) + \sin(\beta_k x)] + \frac{\sin(\beta_k x) - \sinh(\beta_k x)}{\cosh(\beta_k x) - \cos(\beta_k x)} [\cosh(\beta_k x) + \cos(\beta_k x)]. \quad (8)$$

The dynamic equation of motion for the laminated structure is given by:

The subsequent component of the solution pertains to the

$$\frac{d^2 \eta_k(t)}{dt^2} + 2\xi \omega_k \frac{d\eta_k(t)}{dt} + \omega_k^2 \eta_k(t) = f_k(t). \quad (9)$$

modal mechanical response, as elucidated in Equation (9). This response characterizes the behavior and dynamics of the system in terms of the individual vibration modes. This equation encapsulates the time-dependent properties of the modal mechanical response. Within this equation the second derivative of  $\eta_k(t)$  with respect to time, capturing the acceleration or rate of change of the modal response. The term  $2\xi \omega_k \frac{d\eta_k(t)}{dt}$  accounts for the damping effects and describes the rate of energy dissipation in the system. Additionally,  $\omega_k^2 \eta_k(t)$  corresponds to the square of the natural frequency of the  $k$ -th mode multiplied by the modal response, signifying the inherent stiffness of the system. Finally,  $f_k(t)$  denotes the excitation or external force acting on the  $k$ -th mode.

To compute the normal strain, it is necessary to begin by examining the fundamental definition of normal strain. According to this definition, the normal strain can be quantified as:

$$S(x, y, t) = -y k = -y \frac{\partial^2 u(x, t)}{\partial x^2}. \quad (10)$$

Expressed by Equation (10), the strain, denoted as  $S(x, y, t)$ , can be calculated based on the longitudinal elongation. This equation involves the spatial coordinates ( $x$  and  $y$ ) and the temporal variable ( $t$ ). The term  $y$  represents the distance from

the neutral fiber, and the  $\frac{\partial^2 u(x,t)}{\partial x^2}$  corresponds to the second derivative of the displacement function, denoted as  $u$  with respect to the spatial coordinate  $x$ . By evaluating Equation (10), one can determine the normal strain at a specific point in the fiber, taking into account the displacement and its spatial derivatives. The negative sign indicates that the strain is measured as a contraction or compression relative to the initial length of the fiber. This equation serves as a fundamental tool in understanding the mechanical behavior of materials and structures, particularly in scenarios involving elongation and contraction.

The degree of strain experienced by a beam is influenced by both temperature and applied stress. This is why the strain can be expressed as a function of temperature and stress:

$$S = f(\sigma, T), \quad (11)$$

$$dS = \left(\frac{\partial S}{\partial \sigma}\right)_T d\sigma + \left(\frac{\partial S}{\partial T}\right)_\sigma dT. \quad (12)$$

Equation (11) establishes that strain, denoted as  $S$ , is a function of stress ( $\sigma$ ) and temperature ( $T$ ), captured by the function  $f(\sigma, T)$ . In Equation (12), the differential form of strain, denoted as  $dS$ , can be expressed as the sum of two terms.

The first term,  $\left(\frac{\partial S}{\partial \sigma}\right)_T$ , represents the partial derivative of strain with respect to stress, considering temperature as a constant.

The second term,  $\left(\frac{\partial S}{\partial T}\right)_\sigma$ , denotes the partial derivative of strain with respect to temperature, assuming stress remains constant. This equation allows for the assessment of how strain changes with variations in stress and temperature:

$$dS = \frac{d\sigma}{E} + \alpha dTl. \quad (13)$$

To determine the direct strain experienced by the beam, Equation (13) is employed, assuming uniform temperature and linear thermal expansion ( $\alpha$ ). This equation reveals that the differential strain, is the sum of two terms. The first term represents the contribution of stress to the strain, taking into account the material's Young's modulus ( $E$ ). The second term incorporates the effect of temperature change ( $dT$ ) multiplied by the length of the beam ( $l$ ) and the linear thermal expansion coefficient ( $\alpha$ ). These equations offer valuable tools to investigate and quantify the relationship between strain, stress, and temperature in the context of beams.

### 3. Electromechanical modelling

Electromechanical modeling is essential for comprehending the characteristics of piezoelectric materials. Direct piezoelectric effect means the generation of electric charges in certain substances under mechanical load, whereas the inverse piezoelectric effect involves the material's deformation in response to an externally applied electric field. To explain these phenomena, a set of constitutive equations is commonly used. In the context of a piezoelectric transducer, the total strain experienced can be separated into two components: the mechanical strain resulting from mechanical stress and the actuation strain induced by the applied electric voltage. The strain-charge relationships are represented by Equations (14) and (15):

$$D_m = \varepsilon_{ik}^\sigma \psi_k + d_{mi} \sigma_i, \quad (14)$$

$$S_i = s_{ij}^\psi \sigma_j + d_{mi} \psi_m. \quad (15)$$

Equation (14) relates the vector of electric displacement, denoted as  $D_m$ , to the stress vector ( $\sigma_i$ ), through the matrix of piezoelectric coupling coefficients ( $d_{mi}$ ) and the vector of electric field ( $\psi_k$ ) through the vector of electric permittivity at constant stress ( $\varepsilon_{ik}^\sigma$ ). This equation encapsulates the interplay between mechanical force and the electric field-induced in the transducer.

Similarly, Equation (15) describes the relationship between the strain vector,  $S_i$ , the electric field vector,  $\psi$ , and the stress vector. The compliance tensor coefficients,  $s_{ij}$ , and the piezoelectric coupling coefficients,  $d_{mi}$ , are the main piezoelectric properties used to map the strain vector to stress as well as the electric field to the strain, respectively. The indices  $m, k, i, \text{ and } j$  signifies their respective directions. Linear electrical circuit analysis allows us to derive the equation for the piezoelectric transducer with an attached resistor. The piezo component is considered as an electric charge source, and its electrical capacity is determined accordingly. The detailed derivation of Equation 16 can be found in our previous work [12,26].

$$V_p(t) = \frac{\frac{\gamma l_p b_p d_{31} R_z}{C_p \varepsilon_{11}^E} R_z}{\frac{\gamma l_p b_p \varepsilon_{33}^\sigma}{C_p t_p} (1 - k_{31}^2) R_z + \left(1 - \frac{\gamma l_p b_p \varepsilon_{33}^\sigma}{C_p t_p} (1 - k_{31}^2)\right) \sqrt{R_z^2 + \left(\frac{1}{\omega C_p}\right)^2}} S(t), \quad (16)$$

where:

$$k_{31}^2 = \frac{d_{31}^2}{\varepsilon_{11}^E \varepsilon_{33}^\sigma}. \quad (17)$$

$$P = \frac{V_a^2}{R_z} \quad (18)$$

where:

$V_a$  - the root mean square of the voltage generated by the transducer.

The equation (16) provides an expression for the voltage signal  $V_p(t)$  generated by the transducer, considering various parameters and constants. In this equation,  $\gamma$  represents the percentage of surface area of the electrodes in the transducer. It is determined by multiplying the active area of the piezo element by the volume fraction of copper fibers. The quantities  $l_b, b_p,$  and  $t_p$  denote length, width, and thickness of an active part of the transducer.  $d_{31}$  representing the piezoelectric coefficient,  $s_{11}^E$  denoting the compliance property of the transducer,  $C_p$  indicating the capacitance of the transducer,  $R_z$  representing the resistance connected to the transducer externally and,  $\epsilon_{33}^{\sigma}$  - signifying the electric permittivity. By employing equations 14 through 15, one can obtain valuable insights into the voltage signal, power, and their relationship within the transducer system. These equations consider various parameters and characteristics of the transducer, allowing for a comprehensive analysis of its electrical behavior and performance. MFC (Macro Fiber Composite) transducers are pre-manufactured transducers with a form flexible, thin films.

This work specifically focuses on studying the behavior of the laminated MFC piezoelectric transducer under negative temperatures. To achieve this, an advanced testing machine like the Instron Electropuls E10000 was used to apply carefully controlled sinusoidal forces at the specified frequency. Equipped with a thermal chamber capable of operating across an extensive temperature range from -100 to 350 degrees Celsius, this machine ensured precise temperature control during experiments. To ensure accuracy and reliability, a thoroughly prepared composite plate consisting of three MFC (Macro Fiber Composite) elements securely bonded together was utilized for a three-point bending test. The test involved applying a sinusoidal force to the plate, varying its frequency from 5 to 25 Hz in 5 Hz increments.

Throughout the testing procedure, great care was taken to maintain consistent conditions. A constant preset deflection arrow and constant temperature were maintained, minimizing the impact of parameter fluctuations on the results. To manage

and monitor the experiment, a specialized control procedure was developed using the Instron WaveMatrix system. This system precisely regulated the test parameters, ensuring well-defined experimental conditions and enabling accurate data collection.

Moreover, the voltage signals generated by the MFC elements during testing were continuously recorded using a National Instruments recorder, specifically the NI9215 model. These signals underwent real-time monitoring and analysis through the LabView system, configured with a specialized recording procedure. Employing this comprehensive experimental setup and data acquisition approach aims to offer valuable insights into the performance of the laminated MFC piezoelectric transducer under negative temperatures, thereby contributing to the understanding and development of piezoelectric materials for diverse applications.

As depicted in Figure 1, the test setup involved subjecting Integrated MFC piezoelectric transducers to negative temperatures using a thermal chamber while applying controlled sinusoidal force through an electro-pulse wave generator. The test procedure was as follows: the temperature was increased by ten degrees Celsius in each stage before commencing the temperature stabilization step. Following a period of temperature stabilization ( $t_s = 10$  min), the tested piezoelectric transducer underwent concentric sinusoidal loading under displacement control for five different frequencies. For every two minutes of stabilization time, the frequency was incremented by 5 Hz. The process initiated at 0°C and progressed through the temperatures detailed in Table 1 Table 1. The frequency and temperature ranges to which laminated MFC piezoelectric transducers are subjected.

Frequencies to which the system was subjected (Hz)	5	10	15	20	25
Temperatures to which the system was exposed (°C)	0	-10	-20	-30	-40



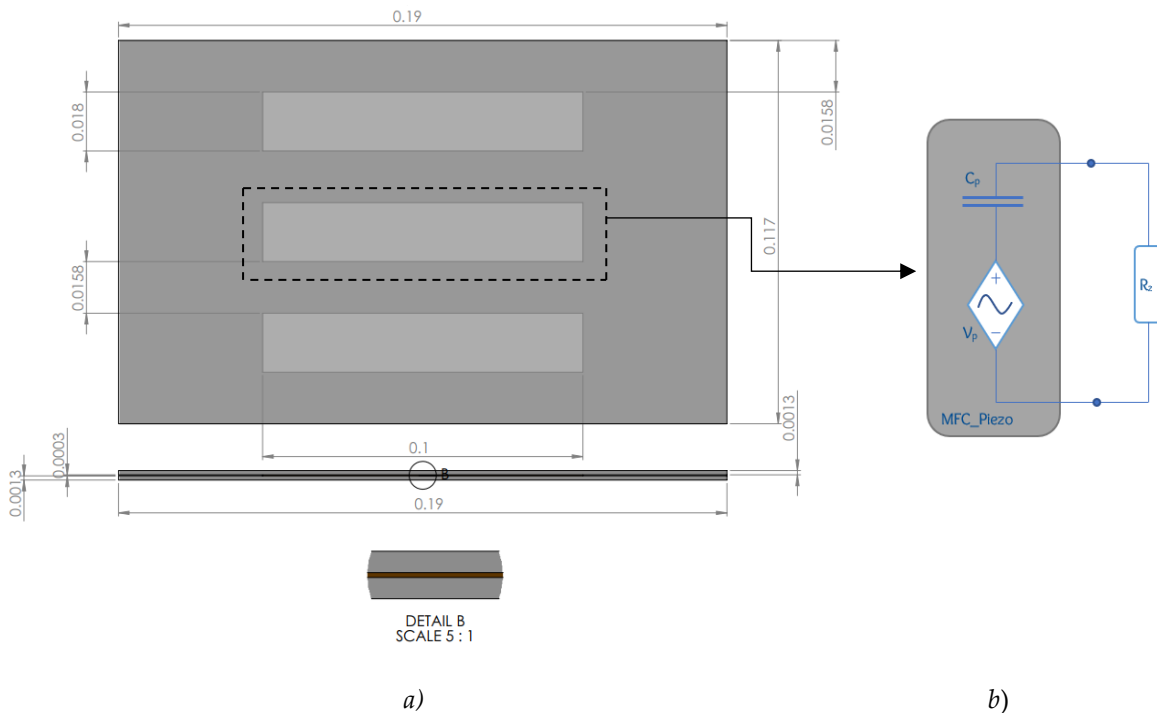
Fig. 1. The test set-up with thermal chamber and excitation system.

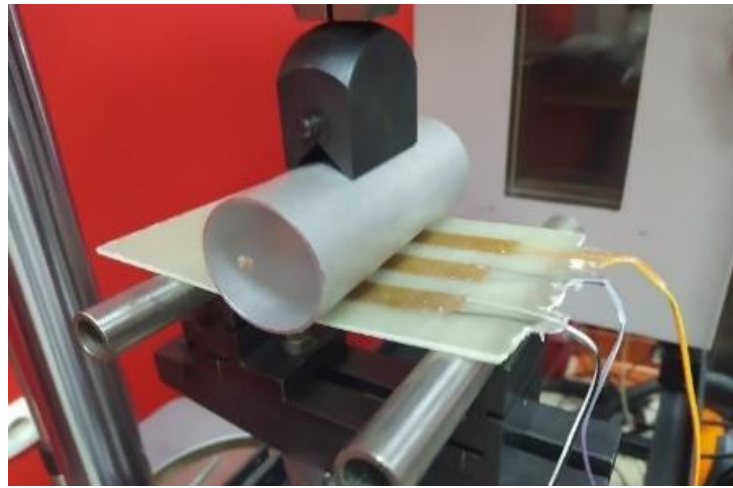
The transducers consisted of multiple layers of piezoceramic material and electrodes, laminated together to form a cohesive structure. The thermal chamber controlled and varied the temperature conditions during the experiments, enabling an analysis of the transducer's performance under diverse thermal conditions. Simultaneously, the electro-pulse wave generator applied cyclic concentric loads, inducing varying levels of stress and strain on the transducers.

The test specimen comprised three MFC piezoelectric transducers (M8514P2 type) integrated within a composite panel. This panel was constructed from a glass fabric with a twill weave, weighing 600 g/m<sup>2</sup>. A separate paper [12] offers

an in-depth description of the system's construction procedure, along with the material properties. This devised solution represents an intelligent structure capable of generating electricity from mechanical vibrations and controlling its dynamic parameters using the laminated piezoelectric transducers.

Figure 2 provides a visual representation of a laminated MFC test sample, serving as a visual reference for the experimental setup employed in the research. The investigation of the piezoelectric transducer's capacitance involved specific methods and materials. The tested MFC transducer's material properties and geometrical parameters are presented in Table 2.





c)

Fig. 2. The MFC (Macro Fiber Composite) piezoelectric transducers are arranged as three parallel samples (a), positioned between epoxy glass fiber composites and (b) an illustrative depiction of the electrical circuit of the piezoelectric transducer, which encompasses an externally attached resistor. The laminated specimen developed for this test (c), in which a concentric cyclic load is supplied using electro-pulse wave generator.

The transducer's terminals were connected to an external resistor placed outside the thermal chamber. To measure the electrical voltage drop across the resistor, a National Instruments measuring card, specifically the NI9215 model capable of monitoring voltage in the range of -10 V to +10 V, was employed. This measuring card was efficiently integrated into the cDAQ-9191 CompactDAQ Chassis and connected to a computer for data collection. The LabVIEW software facilitated the recording and storage of measurement outcomes.

For the testing process, five hundred measurement cycles were designated. To ensure synchronization between data acquisition and the excitation of the test samples, a voltage trigger, produced by the analog output of the Instron controller, was utilized.

Table 2. The tested MFC transducer material properties and geometrical parameters [43]

No.	Description	Notation (Units)	Value
1	Copper fiber volume fraction	$\gamma$ (dimensionless)	0.19
2	Capacity	$C_p(nF)$	84.04
3	PZT fiber thickness	$t_p(\mu m)$	127
4	Active length of MFC	$l_p(mm)$	85
5	Active width of MFC	$b_p(mm)$	14
6	Dielectric constant	$\epsilon_{33}^{\sigma} \left[ \frac{F}{m} \right]$	1.504e-08
7	Elastic compliance constant	$s_{11}^E \left[ \frac{m^2}{N} \right]$	16.4e-12
8	Piezoelectric constant	$d_{31} \left[ \frac{pC}{N} \right]$	-2.1e+2

#### 4. Result and discussion:

The study delves into the impact of negative temperature variations and frequency changes on the sensitivity of an MFC piezoelectric transducer. It scrutinizes the transducer's performance under diverse environmental temperatures and frequencies mirroring real-life surroundings, contributing to the evolution of alternative energy resources. Piezoelectric fiber composites emerge as promising materials for enhancing structural performance across wide temperature ranges. Temperature significantly influences thermoelastic behavior, profoundly affecting the MFC transducer's electric field properties and the laminated system's strain and extension. Both temperature fluctuations and specific frequency-induced loads influence the system's strain. Figure 3 portrays the relationship between transducer strain (displacement) and voltage. The plot indicates a consistent, proportional response, showcasing the transducer's linear conversion capability—from mechanical strain to electrical voltage, as discerned in the analytical study.

It is intriguing that temperature variations consistently induced strain in the MFC transducer, regardless of the frequency parameters. This implies that fluctuations in temperature alone can significantly impact the transducer's strain. Remarkably, substantial displacement or deformation amplified the generation of electric fields (refer to figure 3).

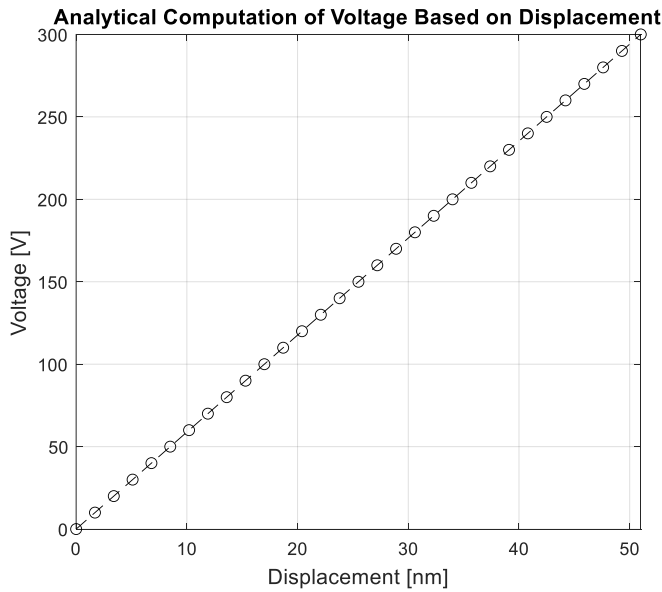


Fig. 3. Theoretical correlation between voltage and transducer displacement, based on equations (14 and 15).

Equation 16 facilitated the calculation of voltage drop across

the external resistance linked to the transducer. In this paper's mathematical model, temperature and frequency stand as independent variables, central to the authors' investigation. Thus, this model proves more valuable and practical compared to previous studies in the field. This research greatly contributes to understanding the sensitivity of MFC transducers, particularly concerning temperature and frequency effects. The findings elucidate the correlation between these parameters and the induced strain within the laminated system.

Figure 4 showcases the theoretical model's voltage predictions, displaying consistent alignment with experimental measurements. The experimental setup involved three MFC piezoelectric transducers integrated into a composite panel made of fiberglass and epoxy resin. Each MFC transducer was connected to an external resistance. The voltage drop across these external resistors was measured, recorded, and then averaged for analysis.

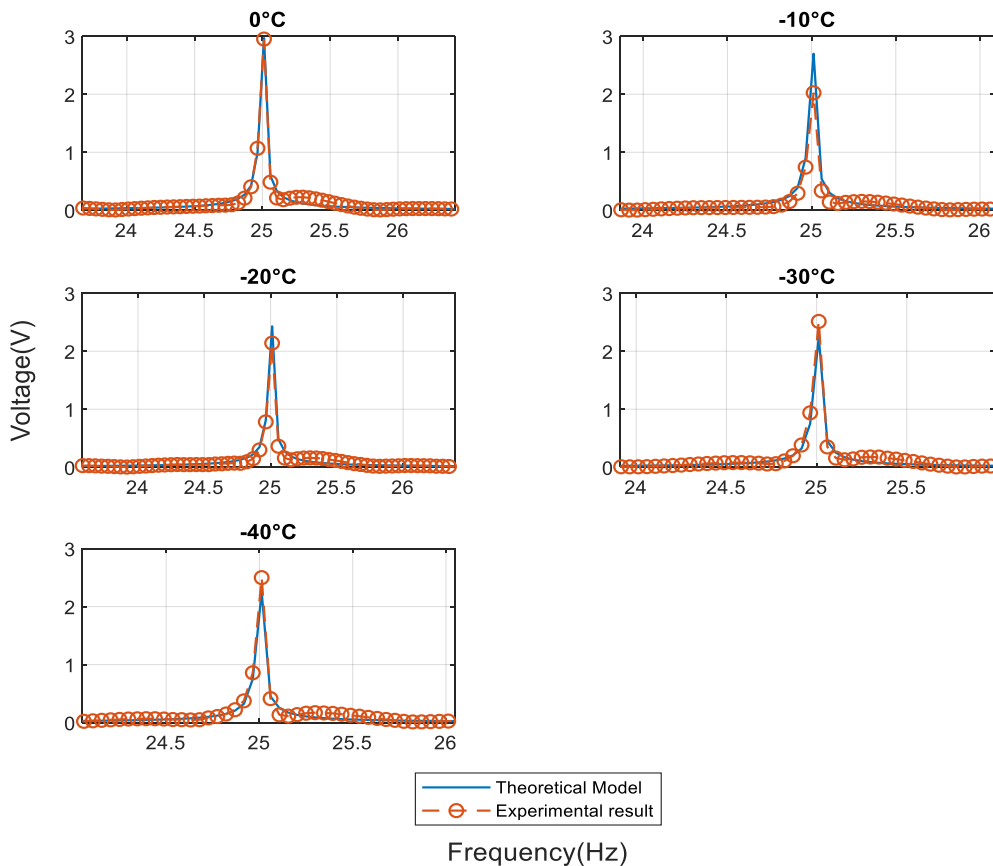


Fig. 4. A correlation between the results obtained from experiments and those generated by model simulations for the voltage measured at various temperature ranges, with a 25 Hz sinusoidal force applied to the transducer.

To simulate real-world conditions, the mathematical model underwent testing across a range of moderate temperature environments, covering both positive and negative temperatures.

This paper delves into temperatures from 0°C to -40°C, while a separate publication examines the range from 25°C to 60°C. The chosen temperature span aims to encapsulate typical

operational scenarios for alternative energy sources, providing an assessment of the MFC transducer's performance within its designated temperature range. The developed mathematical model, expounded in this and previous works [12, 26], exhibited remarkable consistency with experimental results conducted in laboratory settings. This strong alignment between theoretical predictions and actual measurements bolsters the model's reliability. Moreover, the model's efficacy permits the exploration of specific parameters within the energy harvester system when the laminated MFC transducer encounters fluctuations in ambient temperature and frequency.

Figure 5 illustrates the variation in output voltage across diverse temperature and frequency conditions, detailed in reference [12]. In our current investigation, we adopt a similar experimental approach but concentrate on examining negative temperature load conditions. By comparing Figures 4 and 7, it's apparent that the output voltage of the MFC piezoelectric transducer is primarily influenced by temperature and frequency.

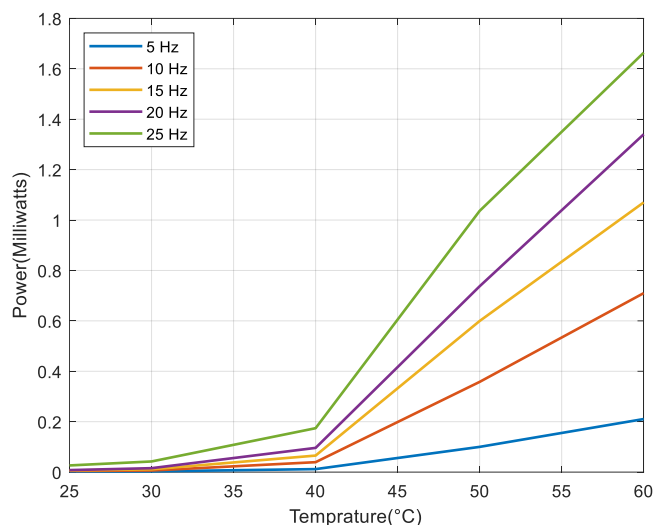


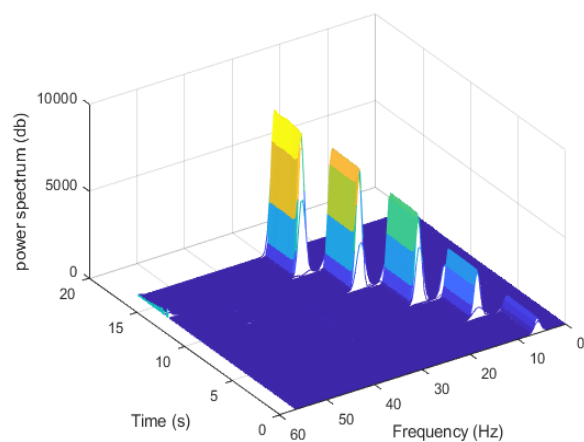
Fig. 5. Power output at various frequencies and temperature ranges based on the reference [12, 26].

In positive temperature conditions, the rate of voltage change demonstrates a more pronounced increase with rising temperatures. Conversely, in negative temperature conditions, the rate of change in output voltage remains relatively constant. This distinction in behavior between positive and negative temperature ranges underscores the distinct sensitivity of the MFC piezoelectric transducer to temperature variations. This observation aligns with trends discussed in existing literature [12, 26], highlighting the transducer's unique response under negative temperature conditions compared to its behavior in

positive temperature ranges. This in-depth analysis of these trends and their implications significantly contributes to our comprehension of the MFC piezoelectric transducer's performance across diverse environmental conditions.

Prior studies [21] extensively explored the behavior of various piezoelectric parameters under different temperatures, including dielectric permittivity, electromechanical coupling factors, and piezoelectric voltage and charge constants. It's been established that temperatures below 150°C have an insignificant impact on these parameters, implying successful transducer application below this temperature threshold without any discernible loss in their piezoelectric properties. However, our research delves deeper and conclusively demonstrates, empirically and theoretically, that the transducer is highly sensitive to temperatures both below and above room temperature. Its efficiency is notably influenced by temperature fluctuations.

a)



b)

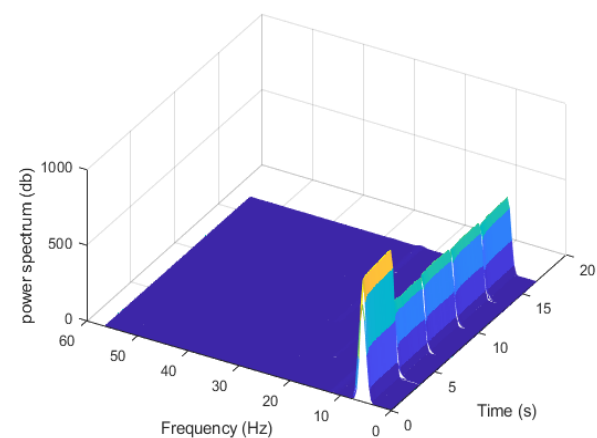


Fig. 6. The 3D spectrogram plot: a – voltage amplitude comparison of the same temperature and different frequency and b – different temperature and the same frequency.

Figure 6 presents a comprehensive analysis of the voltage response using a 3D spectrogram plot. The first part (a) compares voltage amplitudes across different frequencies at a specific temperature, aiming to elucidate how frequency variations affect the voltage output. The second part (b) focuses on comparing voltage amplitudes at various temperatures while maintaining a constant frequency, providing insights into the impact of temperature variations on the voltage response. This spectrogram plot visually encapsulates these comparisons, offering a holistic depiction of the relationship between frequency, temperature, and voltage amplitude.

In Figure 6 -b, the specific experimental conditions entail a constant frequency of 5 Hz within a temperature range from 0°C to -40 degrees Celsius. This plot illustrates the correlation between temperature and voltage amplitude concerning the transducer's performance. Interestingly, the highest voltage amplitude occurred at 0 degrees Celsius, indicating optimal performance at this temperature. Surprisingly, temperatures

below 0 degrees Celsius exhibited a relatively similar impact on the transducer's performance, suggesting that further cooling didn't significantly affect the voltage amplitude. This observation implies that within the studied temperature range, the transducer's performance remained relatively stable and was primarily influenced by the initial temperature drop.

Figure 7 demonstrates the measurement of voltage intensity in the frequency domain across different temperatures. The plot illustrates the relationship between frequency and voltage intensity, depicting how the voltage response varies with different frequencies across the temperature spectrum. Notably, a clear trend emerges where voltage intensity increases with higher excitation frequencies. This discovery indicates that higher excitation frequencies result in a more substantial voltage response from the transducer. The data presented in Figure 8 offers empirical evidence of the system's frequency-dependent behavior and vividly showcases the impact of frequency and temperature on the voltage response.

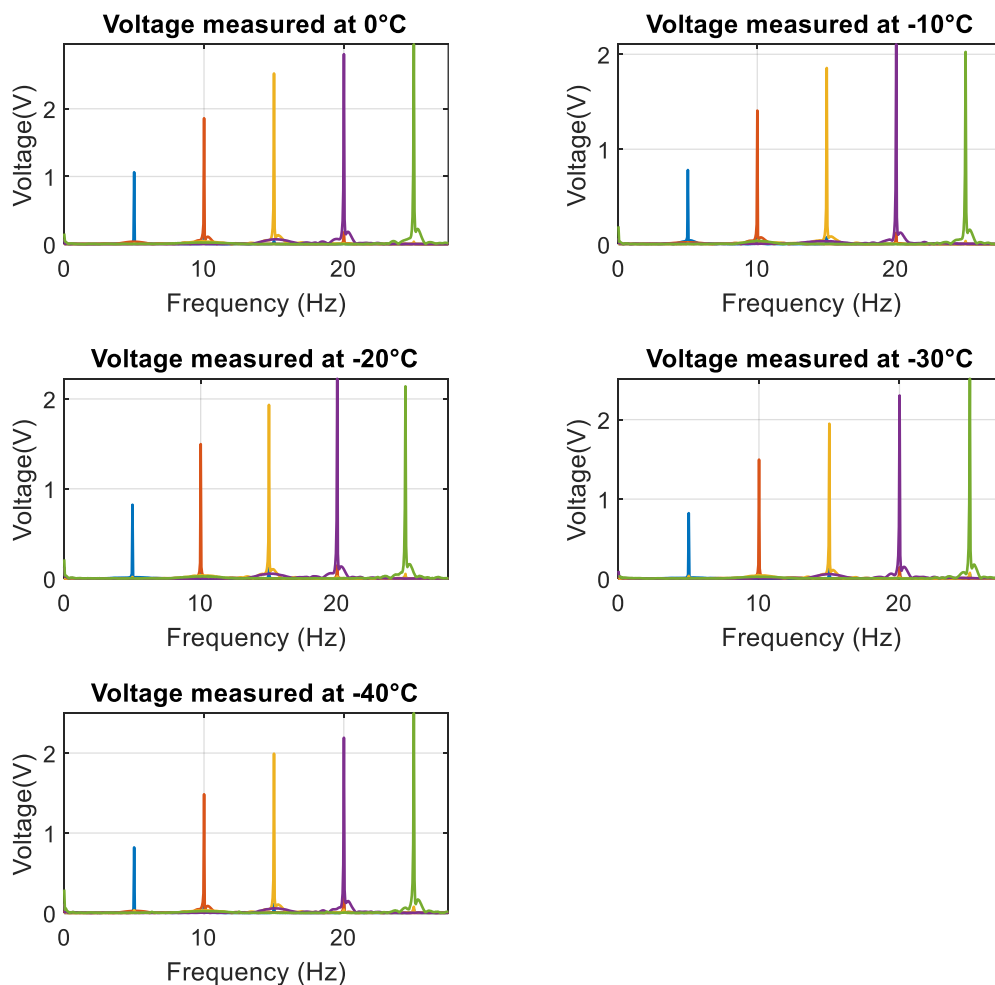


Fig. 7. Measurement of voltage intensity in frequency domain at various temperatures.

An intriguing discovery from this study, in line with references [1, 31], is the substantial variability in sensitivity observed within the moderate temperature range spanning  $-40^{\circ}\text{C}$  to  $+60^{\circ}\text{C}$ . This observation emphasizes the significant influence of temperature fluctuations within this specific range on the transducer's performance. The examination of moderate temperature environments and the analysis of piezoelectric parameters across varying temperatures contribute substantially to comprehending the behavior of the MFC transducer. The observed sensitivity fluctuations within this range hold implications for practical applications, especially in contexts like wireless sensor networks, where consistent and reliable transducer performance is paramount. By delving into and characterizing the transducer's sensitivity within this moderate temperature span, this research offers invaluable insights for refining and optimizing energy harvesting systems in real-world applications, thereby enhancing the reliability and effectiveness of wireless sensor networks.

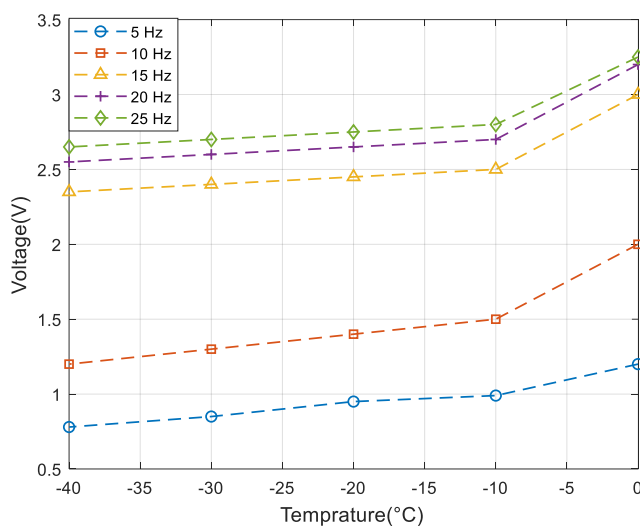


Fig. 8. A summary of voltage measurements taken over a temperature domain at several moderate frequencies.

Figure 8 serves as a comprehensive summary of the generated electric voltage concerning different frequencies across the temperature spectrum. It provides significant insights into how temperature variations correlate with the resulting voltage responses. Noteworthy is the consistent voltage behavior observed in temperatures below 0 degrees Celsius, suggesting a stable response within this temperature range. In contrast, positive temperatures exhibit a remarkable increase in voltage [12]. This observation indicates a more pronounced impact of positive temperatures on voltage behavior, leading to

a substantial voltage rise. The data showcased in Figures 6 and 8 vividly highlights the disparate effects of temperature on voltage response, emphasizing the necessity of considering temperature variations when evaluating the transducer's performance.

## 5. Conclusion

In summary, this study expands upon previous investigations [12], focusing on exploring the impact of sub-zero temperatures and varied frequencies on an MFC piezoelectric transducer. The primary objectives included evaluating the feasibility of utilizing vibrational energy in temperatures below 0 degrees Celsius for powering portable electronic devices in wireless sensor network applications and analyzing the transducer's sensitivity.

### Key Points:

- The developed models underwent validation through experimental measurements, where the MFC piezoelectric transducer was subjected to negative temperature conditions and stress loads.
- Excitation was conducted at low frequencies (5 to 25 Hz) within an operational temperature range of 0 to -40 degrees Celsius, revealing a direct proportional relationship between the electric field properties of the MFC transducer and the strain in the laminated Macro Fiber Composite system.
- Unlike the positive temperature range where sensitivity increased linearly with temperature, the transducer exhibited low sensitivity in the negative range (0 to -40 degrees Celsius) with minimal changes.
- Specifically, at lower frequencies and temperatures between -10 to -40 degrees Celsius, the generated voltage demonstrated consistent characteristics.
- Frequency of excitation emerged as a critical factor influencing the transducer's sensitivity, indicating increased sensitivity at higher frequencies.
- The study underscores the importance of considering temperature and frequency effects when optimizing wireless sensor network systems' performance. The findings suggest potential pathways for sustainable energy solutions.
- This research offers valuable insights into harnessing

vibrational energy in negative temperature environments and holds implications for enhancing power supply and signal measurement mechanisms in low-power electronic devices and wireless sensor networks.

Research on MFC piezoelectric transducers has showcased their versatile applications, from structural monitoring to harvesting energy from mechanical vibrations. Exploring their behavior under diverse temperature and frequency conditions revealed a significant impact of these factors on their performance. The discovery that these transducers respond differently based on temperature ranges, especially in negative conditions, is pivotal for developing efficient energy systems. In positive temperatures, sensitivity increased linearly with temperature rise, while in negative conditions (0 to -40 degrees

Celsius), low sensitivity with minimal changes was observed. Analyzing the effect of vibration frequencies on transducer sensitivity indicated that higher frequencies were linked to increased transducer sensitivity. These studies underscore the importance of considering temperature and frequency effects in optimizing sensor network systems. They also highlight the potential of utilizing mechanical vibrations in low-temperature environments as an energy source, with significant implications for developing efficient power solutions for low-power electronic devices and wireless sensor networks.

These investigations have made a significant contribution to understanding the behavior of MFC piezoelectric transducers in diverse environmental conditions, paving the way for the development of sustainable energy systems capable of harnessing mechanical vibrations in low-temperature settings.

## Reference

1. Ahmed, R. et al.: A review on energy harvesting approaches for renewable energies from ambient vibrations and acoustic waves using piezoelectricity. *Smart Mater. Struct.* 26, 8, 085031 (2017). <https://doi.org/10.1088/1361-665X/aa7bfb>.
2. Aliabadi, M.H.F., Khodaei, Z.S.: *Structural Health Monitoring for Advanced Composite Structures*. World Scientific (2017). <https://doi.org/10.1142/q0114>
3. Appiah, A.N.S. et al.: Hardfacing of mild steel with wear-resistant Ni-based powders containing tungsten carbide particles using powder plasma transferred arc welding technology. *Materials Science-Poland.* 40, 3, 42–63 (2022). <https://doi.org/10.2478/msp-2022-0033>.
4. Appiah, A.N.S. et al.: Powder Plasma Transferred Arc Welding of Ni-Si-B+60 wt%WC and Ni-Cr-Si-B+45 wt%WC for Surface Cladding of Structural Steel. *Materials.* 15, 14, 4956 (2022). <https://doi.org/10.3390/ma15144956>.
5. Banerjee, S. et al.: A critical review on lead-free hybrid materials for next generation piezoelectric energy harvesting and conversion. *Ceramics International.* 47, 12, 16402–16421 (2021). <https://doi.org/10.1016/j.ceramint.2021.03.054>.
6. Borzea, C. et al.: Temperature Influence on the Performances of a PZT-5H Piezoelectric Harvester. In: *2021 12th International Symposium on Advanced Topics in Electrical Engineering (ATEE)*. pp. 1–6 (2021). <https://doi.org/10.1109/ATEE52255.2021.9425102>.
7. Cao, X. et al.: Piezoelectric Nanogenerators Derived Self-Powered Sensors for Multifunctional Applications and Artificial Intelligence. *Adv Funct Materials.* 31, 33, 2102983 (2021). <https://doi.org/10.1002/adfm.202102983>.
8. Choi, H.S.: Architectural Simulation of Hybrid Energy Harvesting: A Design Experiment in Lanzarote Island. *Applied Sciences.* 11, 24, 12146 (2021). <https://doi.org/10.3390/app112412146>.
9. Covaci, C., Gontean, A.: Piezoelectric Energy Harvesting Solutions: A Review. *Sensors.* 20, 12, 3512 (2020). <https://doi.org/10.3390/s20123512>.
10. Degefa, T.G. et al.: Modelling and Study of the Effect of Geometrical Parameters of Piezoelectric Plate and Stack. *Applied Sciences.* 11, 24, 11872 (2021). <https://doi.org/10.3390/app112411872>.
11. Di Rito, G. et al.: Dynamic Modelling and Experimental Characterization of a Self-Powered Structural Health-Monitoring System with MFC Piezoelectric Patches. *Sensors.* 20, 4, 950 (2020). <https://doi.org/10.3390/s20040950>.
12. Degefa, G. T. et al.: The Study of the Influence of Temperature and Low Frequency on the Performance of the Laminated MFC Piezoelectric Energy Harvester. *Applied Sciences.* 12, 23, 12135 (2022). <https://doi.org/10.3390/app122312135>.
13. Gao, S. et al.: High-Performance Wireless Piezoelectric Sensor Network for Distributed Structural Health Monitoring. *International Journal of Distributed Sensor Networks.* 12, 3, 3846804 (2016). <https://doi.org/10.1155/2016/3846804>.
14. Gholikhani, M. et al.: A critical review of roadway energy harvesting technologies. *Applied Energy.* 261, 114388 (2020).

<https://doi.org/10.1016/j.apenergy.2019.114388>.

15. Grzybek, D., Micek, P.: Piezoelectric beam generator based on MFC as a self-powered vibration sensor. *Sensors and Actuators A: Physical*. 267, 417–423 (2017). <https://doi.org/10.1016/j.sna.2017.10.053>.
16. Hirst, J. et al.: Long-term power degradation testing of piezoelectric vibration energy harvesters for low-frequency applications. *Eng. Res. Express*. 2, 3, 035026 (2020). <https://doi.org/10.1088/2631-8695/abaf09>.
17. Jasim, M.H. et al.: Analytical analysis of jute–epoxy beams subjected to low-velocity impact loading. *International Journal of Structural Integrity*. 12, 3, 428–438 (2020). <https://doi.org/10.1108/IJSI-04-2020-0037>.
18. Karadimas, G., Salonitis, K.: Ceramic Matrix Composites for Aero Engine Applications—A Review. *Applied Sciences*. 13, 5, 3017 (2023). <https://doi.org/10.3390/app13053017>.
19. Kargar, S.M., Hao, G.: An Atlas of Piezoelectric Energy Harvesters in Oceanic Applications. *Sensors*. 22, 5, 1949 (2022). <https://doi.org/10.3390/s22051949>.
20. Manish, Sukesh: Piezoelectric energy harvesting in wireless sensor networks. In: 2015 2nd International Conference on Recent Advances in Engineering & Computational Sciences (RAECS). pp. 1–6 (2015). <https://doi.org/10.1109/RAECS.2015.7453339>.
21. Miclea, C. et al.: Effect of temperature on the main piezoelectric parameters of a soft PZT ceramic. *ROMANIAN JOURNAL OF INFORMATION SCIENCE AND TECHNOLOGY*. 10, 243–250 (2007).
22. Mouapi, A. et al.: Autonomous Wireless Sensors Network Based on Piezoelectric Energy Harvesting. *Open Journal of Antennas and Propagation*. 4, 3, 138–157 (2016). <https://doi.org/10.4236/ojapr.2016.43011>.
23. Nabavi, S.F. et al.: An ocean wave-based piezoelectric energy harvesting system using breaking wave force. *International Journal of Mechanical Sciences*. 151, 498–507 (2019). <https://doi.org/10.1016/j.ijmecsci.2018.12.008>.
24. Nastro, A. et al.: Wearable Ball-Impact Piezoelectric Multi-Converters for Low-Frequency Energy Harvesting from Human Motion. *Sensors*. 22, 3, 772 (2022). <https://doi.org/10.3390/s22030772>.
25. Nguyen, V.-C. et al.: Printing smart coating of piezoelectric composite for application in condition monitoring of bearings. *Materials & Design*. 215, 110529 (2022). <https://doi.org/10.1016/j.matdes.2022.110529>.
26. Płaczek, M., Kokot, G.: Modelling and Laboratory Tests of the Temperature Influence on the Efficiency of the Energy Harvesting System Based on MFC Piezoelectric Transducers. *Sensors (Basel)*. 19, 7, 1558 (2019). <https://doi.org/10.3390/s19071558>.
27. Qian, H.-M. et al.: Structural fatigue reliability analysis based on active learning Kriging model. *International Journal of Fatigue*. 172, 107639 (2023). <https://doi.org/10.1016/j.ijfatigue.2023.107639>.
28. Qian, H.-M. et al.: Time-Variant Reliability Analysis for a Complex System Based on Active-Learning Kriging Model. *ASCE-ASME Journal of Risk and Uncertainty in Engineering Systems, Part A: Civil Engineering*. 9, 1, 04022055 (2023). <https://doi.org/10.1061/AJRUA6.RUENG-962>.
29. Qing, X. et al.: Piezoelectric Transducer-Based Structural Health Monitoring for Aircraft Applications. *Sensors*. 19, 3, 545 (2019). <https://doi.org/10.3390/s19030545>.
30. Qing, X.P. et al.: Built-in Sensor Network for Structural Health Monitoring of Composite Structure. *Journal of Intelligent Material Systems and Structures*. 18, 1, 39–49 (2007). <https://doi.org/10.1177/1045389X06064353>.
31. Ramírez, J.M. et al.: Energy harvesting for autonomous thermal sensing using a linked E-shape multi-beam piezoelectric device in a low frequency rotational motion. *Mechanical Systems and Signal Processing*. 133, 106267 (2019). <https://doi.org/10.1016/j.ymsp.2019.106267>.
32. Randriantsoa, A.N.A. et al.: Recent Advances in Hybrid Energy Harvesting Technologies Using Roadway Pavements: A Review of the Technical Possibility of Using Piezo-thermoelectrical Combinations. *Int. J. Pavement Res. Technol.* (2022). <https://doi.org/10.1007/s42947-022-00164-z>.
33. Ravikumar, C., Markevicius, V.: Development of Ultrasound Piezoelectric Transducer-Based Measurement of the Piezoelectric Coefficient and Comparison with Existing Methods. *Processes*. 11, 8, 2432 (2023). <https://doi.org/10.3390/pr11082432>.
34. Salazar, R. et al.: Fatigue in piezoelectric ceramic vibrational energy harvesting: A review. *Applied Energy*. 270, 115161 (2020). <https://doi.org/10.1016/j.apenergy.2020.115161>.
35. Sathiyamoorthy, S., Bharathi, N.: Hybrid Energy Harvesting using Piezoelectric Materials, Automatic Rotational Solar Panel, Vertical Axis

- Wind Turbine. *Procedia Engineering*. 38, 843–852 (2012). <https://doi.org/10.1016/j.proeng.2012.06.106>.
36. Snopiński, P. et al.: Investigation of Microstructure and Mechanical Properties of SLM-Fabricated AlSi10Mg Alloy Post-Processed Using Equal Channel Angular Pressing (ECAP). *Materials*. 15, 22, 7940 (2022). <https://doi.org/10.3390/ma15227940>.
  37. Sun, C. et al.: On Piezoelectric Energy Harvesting from Human Motion. *Journal of Power and Energy Engineering*. 7, 1, 155–164 (2019). <https://doi.org/10.4236/jpee.2019.71008>.
  38. Wang, S. et al.: Fatigue life prediction of composite suspension considering residual stress and crack propagation. *Proceedings of the Institution of Mechanical Engineers, Part D: Journal of Automobile Engineering*. 237, 6, 1299–1312 (2023). <https://doi.org/10.1177/09544070221091683>.
  39. Xie, X.D. et al.: Energy harvesting from transverse ocean waves by a piezoelectric plate. *International Journal of Engineering Science*. 81, 41–48 (2014). <https://doi.org/10.1016/j.ijengsci.2014.04.003>.
  40. Yang, Y. et al.: Vibration energy harvesting using macro-fiber composites. *Smart Mater. Struct.* 18, 11, 115025 (2009). <https://doi.org/10.1088/0964-1726/18/11/115025>.
  41. An Active Diagnostic System for Structural Health Monitoring of Rocket Engines - Xinlin P. Qing, Hian-Leng Chan, Shawn J. Beard, Amrita Kumar, 2006, <https://journals.sagepub.com/doi/abs/10.1177/1045389X06059956?journalCode=jima>, last accessed 2023/05/11.
  42. Composite Material - an overview | ScienceDirect Topics, <https://www.sciencedirect.com/topics/social-sciences/composite-material>, last accessed 2023/07/01.
  43. MacroFiberComposite™, <https://www.smart-material.com/MFC-product-mainV2.html>, last accessed 2023/12/09.
  44. Piezoelectric Effect - an overview | ScienceDirect Topics, <https://www.sciencedirect.com/topics/engineering/piezoelectric-effect>, last accessed 2023/05/11.
  45. Piezoelectric energy harvesting for self-powered wearable upper limb applications - Liu - 2021 - *Nano Select* - Wiley Online Library, <https://onlinelibrary.wiley.com/doi/full/10.1002/nano.202000242>, last accessed 2023/05/11.